

# The square lattice Ising model with quenched surface disorder

Luca Cervellera<sup>1</sup>, Oliver Oing<sup>1</sup>, Jan BÜddefeld<sup>1</sup> and Alfred Hucht<sup>1\*</sup>

<sup>1</sup> Fakultät für Physik, Universität Duisburg-Essen and CENIDE, D-47048 Duisburg, Germany

\* fred@thp.uni-due.de

## Abstract

Using exact enumeration, the Casimir amplitude and the Casimir force are calculated for the square lattice Ising model with quenched surface disorder on one surface in cylinder geometry at criticality. The system shape is characterized by the aspect ratio  $\rho = L/M$ , where the cylinder length  $L$  can take arbitrary values, while the circumference  $M$  is varied from  $M = 4$  to  $M = 54$ , resulting in up to  $2^{54}$  numerically exact free energy calculations. A careful  $M \rightarrow \infty$  extrapolation shows that quenched surface disorder is irrelevant in two dimensions, but gives rise to logarithmic corrections.

Copyright attribution to authors.

This work is a submission to SciPost Physics.

License information to appear upon publication.

Publication information to appear upon publication.

Received Date

Accepted Date

Published Date

## 1 Introduction

The square lattice Ising model [1] is often referred to as the drosophila of statistical physics. It is one of the few exactly solvable models that has a continuous phase transition at finite temperatures. After the seminal exact solution on the torus by Onsager and Kaufman [2, 3], which lead to the exact bulk free energy density  $f_b(T)$ , several other geometries and boundary conditions (BCs) were examined. Using the dimer representation by Kasteleyn [4, 5] and its generalization by Fisher [6], McCoy and Wu derived an exact solution on the cylinder [7, 8], and gave exact expressions for the surface free energy density  $f_s^{(o)}(T)$  for an open boundary, as well as in a surface magnetic field. Motivated by the universal critical Casimir effect [9], which describes the attraction or repulsion of boundaries enclosing a correlated medium similar to the quantum electrodynamical Casimir effect [10], several other BCs were studied [11, 12].

Apart from that, progress was made towards an exact solution of the Ising model without periodic BCs in either direction. This solution turned out to be quite involved, because no Fourier transformation could be used in at least one direction. In two completely independent works, Baxter [13] and Hucht [14–16] derived explicit expressions for the partition function of the Ising model on the rectangle. While Baxter used the spinor method by Kaufman and focused on the surface and corner free energy contributions, verifying a conjecture for the corner contributions by Vernier and Jacobsen [17], Hucht utilized the dimer method combined with block transfer matrices [18] and focused on the universal Casimir contributions in this system.

The method established in [14–16] turned out to be applicable to other BCs, as well as to disordered systems [19–22]. In this work, it will be used to calculate the partition function and free energy of a cylinder of length  $L$  and circumference  $M$  with open BCs at the left side and arbitrary fixed BCs at the right side. By averaging the free energy over the  $2^M$  possible

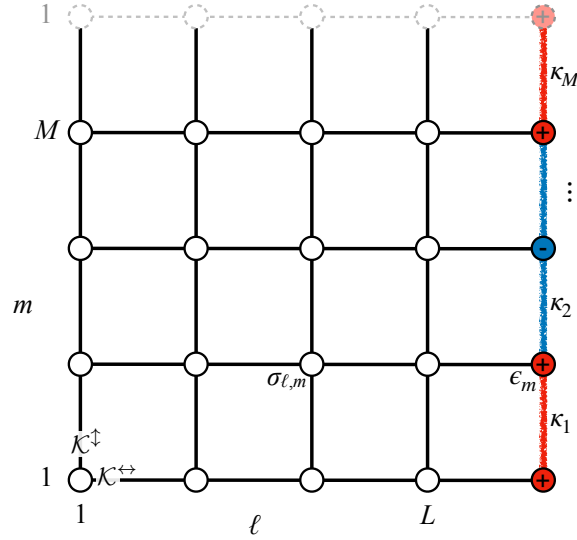


Figure 1: The system.

boundary configurations, the quenched disorder average is obtained. In this way, we can test several predictions for this system [23, 24]. We remark that our exact approach is orders of magnitude faster than the Monte-Carlo simulations performed by Pleimling and coworkers [25], as we can determine the numerically exact free energy of a system with size  $M \times L$  in  $\mathcal{O}(M)$  steps using the principal minor algorithm by Griffin and Tsatsomeros [26], while the Monte-Carlo approach required a full simulation for each boundary configuration. The principal minor algorithm has also been successfully applied recently to diagrammatic Monte Carlo quantum simulations [27].

## 2 Model and method

### 2.1 Partition function for quenched surface disorder

The system under consideration is the anisotropic square lattice Ising model on a cylinder with length  $L$  and circumference  $M$ , as shown in Fig. 1. Neighboring Ising spins  $\sigma_{l,m} = \pm 1$  interact via the reduced couplings  $K^{\leftrightarrow, \uparrow, \downarrow}$  in the two directions. While the left side of the cylinder has open (o) boundary conditions (BCs) for simplicity, at the right side we assume quenched random disordered (r) BCs, where the surface spins  $\sigma_{L,m}$  in layer  $L$  couple to frozen fixed boundary spins  $\epsilon_m = \pm 1$  in the additional boundary layer  $L + 1$ , with coupling strength  $K_s^{\leftrightarrow}$ . Note that this boundary layer acts like a quenched random surface field of strength  $K_s^{\leftrightarrow}$ . Unless otherwise stated, we assume  $K_s^{\leftrightarrow} = K^{\leftrightarrow}$ .

As we can neither apply symmetry breaking fields nor set certain spins to fixed values in the exact calculation of the partition function, we instead add an additional coupling term to the Hamiltonian, that couples the boundary spins  $\epsilon_m$  infinitely strong as required, using the corresponding bond disorder variables  $\kappa_m$  fulfilling  $\kappa_m = \epsilon_m \epsilon_{m+1}$ . Note that due to the periodic boundary condition in  $\uparrow$ -direction,  $\sum_m \kappa_m$  must be even, such that there are  $M - 1$  independent disorder degrees of freedom  $\kappa_1, \dots, \kappa_{M-1}$ . We write  $\vec{\kappa} = \{\kappa_1, \dots, \kappa_{M-1}, 0\}$  for the disorder configuration, where the zero at position  $M$  is added for later convenience. The

reduced Hamiltonian is therefore given by

$$\begin{aligned} \mathcal{H}^{(o,r)}(\vec{\kappa}) = & -K^{\leftrightarrow} \sum_{l=1}^{L-1} \sum_{m=1}^M \sigma_{l,m} \sigma_{l+1,m} - K^{\updownarrow} \sum_{l=1}^L \sum_{m=1}^M \sigma_{l,m} \sigma_{l,m+1} \\ & - K_s^{\leftrightarrow} \sum_{m=1}^M \sigma_{L,m} \epsilon_m - \lim_{K_s^{\updownarrow} \rightarrow \infty} K_s^{\updownarrow} \sum_{m=1}^{M-1} (\kappa_m \epsilon_m \epsilon_{m+1} - 1). \end{aligned} \quad (1)$$

First we discuss two special cases: for  $\kappa_m = +1$  all boundary spins  $\epsilon_m$  are forced to be parallel, which corresponds to the well known plus ( $\epsilon_m = +1$ ) or minus ( $\epsilon_m = -1$ ) boundary conditions. On the other hand, the case  $\kappa_m = -1$  resembles the two possible staggered boundary conditions ( $\epsilon_m = \pm(-1)^m$ ), which are known to be in the Dirichlet surface universality class [28].

As the focus of this work is on critical systems, it is useful to describe the couplings in the following as  $z = \tanh K^{\leftrightarrow}$  and  $t = e^{-2K^{\updownarrow}}$ . Then, the critical point is at

$$t = z, \quad (2)$$

where the isotropic case  $K^{\leftrightarrow} = K^{\updownarrow}$  is given by the coupling  $z_c^{\text{iso}} = \sqrt{2} - 1$ , which was originally calculated by Kramers and Wannier [29]. In addition to this isotropic critical point we also consider the Hamiltonian limit [30], where  $t, z \nearrow z_c^{\text{hl}} = 1$ .

The partition function for a system with an arbitrary, quenched boundary condition

$$Z^{(o,r)}(L, M; \vec{\kappa}) = \sqrt{C \det \langle \mathbf{e}_o | \mathcal{T}^L | \mathbf{e}_\kappa \rangle}, \quad (3)$$

can be calculated with a transfer-matrix method, with  $2M \times 2M$  transfer matrix  $\mathcal{T}$ , similar to the case for open boundaries [14–16]. The open and the quenched boundary condition of the considered system are described by the  $2M \times M$  block vectors  $|\mathbf{e}_o\rangle$  and  $|\mathbf{e}_\kappa\rangle$ , respectively. The detailed derivation of the partition function is shown in the appendix A.

## 2.2 Disorder ensembles and the free energy

In the presence of quenched disorder, the reduced free energy (in units of  $k_B T$ ),

$$F^{(o,r)}(L, M; \vec{\kappa}) = -\log Z^{(o,r)}(L, M; \vec{\kappa}), \quad (4)$$

has to be averaged over the disorder ensemble  $\{\kappa\}$  according to

$$\bar{F}^{(o,r)}(L, M) = \langle F^{(o,r)}(L, M; \vec{\kappa}) \rangle_\kappa = \frac{\sum_{\{\kappa\}} F^{(o,r)}(L, M; \vec{\kappa})}{\sum_{\{\kappa\}} 1} \quad (5)$$

in order to get the proper disorder-averaged free energy [31]. In this work, we will distinguish different disorder ensembles, discriminated by the boundary magnetization

$$m_B(\vec{\kappa}) = \frac{M_B(\vec{\kappa})}{M} = \frac{1}{M} \sum_{m=1}^M \epsilon_m \quad (6)$$

of the random surface: (i) the free ensemble average  $\langle \cdot \rangle_\kappa$  runs over all  $2^M$  disorder configurations, such that  $-1 \leq m_B(\vec{\kappa}) \leq 1$ , while (ii) the ensemble  $\langle \cdot \rangle_\kappa^{(m_B=0)}$  is restricted to configurations with fixed  $m_B(\vec{\kappa}) = 0$ . Note that in both cases  $\bar{m}_B = 0$ . Also, (iii) ensembles with fixed  $m_B(\vec{\kappa})$  to other values than zero are denoted similarly.

Alternatively to (5), we can introduce the density of thermodynamic states (DOTS),

$$\omega^{(o,r)}(L, M; F, M_B) = \langle \delta[F^{(o,r)}(L, M; \vec{\kappa}) - F] \delta[M_B(\vec{\kappa}) - M_B] \rangle_{\kappa}, \quad (7)$$

with Dirac's delta distribution  $\delta(x)$ , to get

$$\bar{F}^{(o,r)}(L, M) = \int dF \int dM_B F \omega^{(o,r)}(L, M; F, M_B). \quad (8)$$

In the following, we will analyze DOTs like (7) instead of simple averages (5).

### 2.3 The excess free energy

As shown in the appendix, we can factorize the  $M \times M$  matrix in the partition function (3) according to

$$\langle \mathbf{e}_o | \mathcal{T}^L | \mathbf{e}_\kappa \rangle = \mathbf{P}(\mathbf{Q} + \boldsymbol{\kappa}),$$

where  $\mathbf{P}$  contains contributions from the bulk and the open boundary,  $\mathbf{Q}$  is a skew-circulant matrix convergent in the limit  $L, M \rightarrow \infty$ , and  $\boldsymbol{\kappa} = \text{diag}(\vec{\kappa})$  contains the disorder. Hence we can define the excess free energy relative to the staggered case  $\kappa_m = -1$ ,

$$F^{(\text{ex})}(L, M; \vec{\kappa}) = F^{(o,r)}(L, M; \vec{\kappa}) - F^{(o,\uparrow)}(L, M) \quad (9a)$$

$$= -\frac{1}{2} \log \det(\mathbf{Q} + \boldsymbol{\kappa}) + \frac{1}{2} \log \det(\mathbf{Q} - \mathbf{1}), \quad (9b)$$

where  $F^{(o,\uparrow)}(L, M) = F^{(o,r)}(L, M; -\vec{1})$  is the free energy of a system with an open boundary on one side and a staggered boundary on the other side.

The resulting distribution function of  $F^{(\text{ex})}$  is related to the DOTs (7) of  $F$  via a simple shift by the constant  $F^{(o,\uparrow)}(L, M)$ ,

$$\omega^{(\text{ex})}(L, M; F^{(\text{ex})}, M_B) = \omega(L, M; F, M_B), \quad (10)$$

where the free variables are related according to (9a),  $F^{(\text{ex})} = F - F^{(o,\uparrow)}(L, M)$ . The resulting distribution function for  $M = 40$  and  $L \rightarrow \infty$ , containing  $2^{40}$  exact free energies, is shown in Fig. 2. To get a little intuition for this density of thermodynamic states, some distinguished spin configurations are marked in the figure. From Fig. 2 we can read off the two extremal cases,

$$\max_{\vec{\kappa}} F(L, M; \vec{\kappa}) = F^{(o,\uparrow)}(L, M), \quad (11a)$$

$$\min_{\vec{\kappa}} F(L, M; \vec{\kappa}) = F^{(o,+)}(L, M), \quad (11b)$$

such that  $F^{(\text{ex})}(L, M; \vec{\kappa}) \leq 0$  for all  $\vec{\kappa}$ .

### 2.4 Residual free energy and scaling limit

In the thermodynamic limit  $L, M \rightarrow \infty$ , the average free energy (5) diverges and needs to be regularized to get the finite residual free energy

$$\delta \bar{F}^{(o,r)}(L, M) = \bar{F}^{(o,r)}(L, M) - \bar{F}_{\infty}^{(o,r)}(L, M). \quad (12)$$

The leading divergence  $\bar{F}_{\infty}$  contains the bulk and surface free energies of the system,

$$\bar{F}_{\infty}^{(o,r)}(L, M) = LM f_b + M(f_s^{(o)} + \bar{f}_s^{(r)}), \quad (13)$$

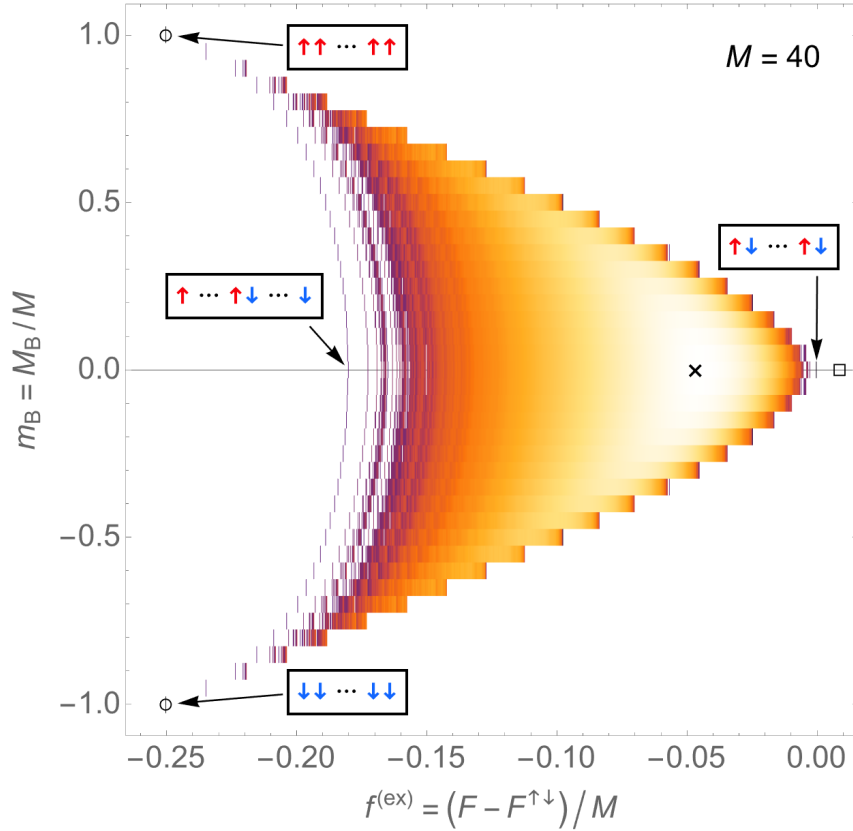


Figure 2: Density of thermodynamic states (10), with excess free energy density  $f^{(\text{ex})}$  and boundary magnetisation  $m_B$ , for a lattice with  $M = 40$ ,  $L \rightarrow \infty$  and isotropic couplings  $z = t = z_c^{\text{iso}}$  at criticality. Exact calculations were done for all  $2^M$  surface disorder configurations, with distinguished surface configurations pointed out in the figure. Also marked are the surface free energies  $f_s^{(+)}(z_c^{\text{iso}})$ ,  $f_s^{(\uparrow\downarrow)}(z_c^{\text{iso}})$  and  $\bar{f}_s^{(r)}(z_c^{\text{iso}})$  from Eqs. (15a) as  $(\circ)$ ,  $(\square)$  and  $(\times)$ , respectively.

where the random boundary needs to be disorder averaged in order to get a well defined limit for the random surface free energy density,

$$\bar{f}_s^{(r)} = -f_s^{(o)} + \lim_{M \rightarrow \infty} \frac{1}{M} [\bar{F}^{(o,r)}(L, M) - LM f_b]. \quad (14)$$

While the bulk free energy density  $f_b$  and the surface free energy densities for open, staggered and fixed surfaces are known exactly both at and away from criticality [8, 28, 32, 33], the random surface free energy (14) will be calculated numerically in section 3.2 and is listed here for reference. The critical values are

$$f_b(z_c) = \begin{cases} \frac{1}{2} \log \frac{-(z_c)}{2} - \frac{1}{2\pi} \int_0^\pi \gamma d\varphi & \text{if } z_c < 1 \\ -\log 2 - \frac{\gamma_{EM}}{2} & z_c \rightarrow 1 \end{cases} \quad (15a)$$

$$f_s^{(o)}(z_c) = \begin{cases} -\frac{\log(\frac{1-z_c^2}{4})}{4} - \frac{1}{4\pi} \int_0^\pi \log[1 + \sin \omega] d\varphi & \text{if } z_c < 1 \\ \frac{\log 2}{2} - \frac{G}{\pi} - \frac{\gamma_{EM}}{4} & z_c \rightarrow 1 \end{cases} \quad (15b)$$

$$\bar{f}_s^{(r)}(z_c) = \begin{cases} 0.002662(25 \pm 28) & \text{if } z_c = z_c^{\text{iso}} \\ 0.26536(96 \pm 10) & z_c \rightarrow 1 \end{cases} \quad (15c)$$

$$f_s^{(m_B=0)}(z_c^{\text{iso}}) = 0.00266(42 \pm 20) \quad (15d)$$

with Euler-Mascheroni constant  $\gamma_{\text{EM}}$  and Catalan's constant  $G$ . Note that for  $f_b(1)$  and  $f_s^{(o)}(1)$ , the regularization  $\sum_{k=1}^{\infty} k^{-1} = \gamma_{\text{EM}}$  is used and the angles  $\gamma$ ,  $\omega$  and  $\varphi$  are introduced (B.3) in the appendix.

In the scaling limit, with fixed aspect ratio  $\rho = L/M$ , the average residual free energy (12) at criticality becomes asymptotically equal to the Casimir amplitude of the considered boundary conditions,

$$\Delta_{\text{C}}^{(o,r)}(\rho) \simeq \delta \bar{F}^{(o,r)}(L, M). \quad (16)$$

The corresponding average residual excess free energy (9a) is then given by

$$\delta \bar{F}^{(\text{ex})}(L, M) = \bar{F}^{(\text{ex})}(L, M) - \bar{F}_{\infty}^{(\text{ex})}(L, M), \quad (17a)$$

$$\bar{F}_{\infty}^{(\text{ex})}(L, M) = M(f_s^{(r)} - f_s^{(\uparrow\downarrow)}), \quad (17b)$$

fulfilling

$$\Delta_{\text{C}}^{(\text{ex})}(\rho) \simeq \delta \bar{F}^{(\text{ex})}(L, M) \quad (18)$$

in the scaling limit. Note that the bulk contributions in (17b) cancel out.

In addition to (18), the surface disorder averaged Casimir amplitude is given by

$$\Delta_{\text{C}}^{(o,r)}(\rho) = \Delta_{\text{C}}^{(o,\uparrow\downarrow)}(\rho) + \Delta_{\text{C}}^{(\text{ex})}(\rho), \quad (19)$$

with  $\Delta_{\text{C}}^{(o,\uparrow\downarrow)}(\rho)$  as Casimir amplitude for a system with open boundary on one side and staggered boundary condition on the other. Horecht derived a formula for the Casimir amplitude with open boundaries on both sides

$$\Delta_{\text{C}}^{(o,o)}(\rho) = -\frac{\pi\rho}{12} - \log \frac{(-1, e^{-2\pi\rho})_{\infty}}{(-1, e^{-4\pi\rho})_{\infty}} = \log \frac{\eta(i\rho)\eta(4i\rho)}{\eta(2i\rho)^2}, \quad (20)$$

and showed that  $\Delta_{\text{C}}^{(o,\uparrow\downarrow)}(\rho) \equiv \Delta_{\text{C}}^{(o,o)}(\rho)$  is in the Dirichlet surface universality class [28]. In (20),  $(\dots)_{\infty}$  denotes the q-Pochhammer symbol and  $\eta(x)$  stands for the Dedekind eta function. Note that the relation  $\eta(-\frac{1}{x}) = \sqrt{-ix} \eta(x)$  leads to the non-trivial symmetry for the Casimir amplitude with open boundaries

$$\Delta_{\text{C}}^{(o,o)}(\rho) = \Delta_{\text{C}}^{(o,o)}\left(\frac{1}{4\rho}\right). \quad (21)$$

The other well known surface universality class is (o, +), with corresponding Casimir amplitude [28]

$$\Delta_{\text{C}}^{(o,+)}(\rho) = \Delta_{\text{C}}^{(o,o)}(\rho) + \frac{\log 2}{2} - \log \frac{(e^{-2\pi\rho}, e^{-4\pi\rho})_{\infty}}{(-e^{-2\pi\rho}, e^{-4\pi\rho})_{\infty}}. \quad (22)$$

Note that not only the boundary with all spins up, but also the one with all spins down is in this universality class due to the  $Z_2$ -symmetry. Further, boundaries like first-half spins up, second-half down belong in this class too [34].

### 2.4.1 Casimir force

With the free energy as thermodynamic potential, a number of different quantities are now accessible. In the following, we look at the critical Casimir force in  $L$ -direction [35]

$$\mathcal{F}_{\text{C}}(L, M; \vec{\kappa}) = -\frac{1}{M} \frac{\partial}{\partial L} F(L, M; \vec{\kappa}), \quad (23)$$

with corresponding scaling function

$$\vartheta(\rho) = -\rho \frac{\partial}{\partial \rho} \Delta_c(\rho) \cong LM \bar{\mathcal{F}}_c(L, M) \quad (24)$$

in the thermodynamic limit  $L, M \rightarrow \infty$ . At criticality, where we restricted our calculations to, the force becomes significant for different applications, such as colloidal aggregation [36].

We declare the matrix  $\mathbf{G}(\boldsymbol{\kappa})$  as the matrix dual of  $\boldsymbol{\kappa}\mathbf{Q}$ ,

$$\mathbf{G}(\boldsymbol{\kappa}) = \frac{\mathbf{1} - \boldsymbol{\kappa}\mathbf{Q}}{\mathbf{1} + \boldsymbol{\kappa}\mathbf{Q}}. \quad (25)$$

With that, the excess Casimir force is given by

$$\mathcal{F}_c^{(\text{ex})}(L, M; \vec{\kappa}) = -\frac{1}{M} \frac{\partial}{\partial L} F^{(\text{ex})}(L, M; \vec{\kappa}) = \frac{1}{2M} \text{Tr} \left[ \left( \mathbf{G}(\boldsymbol{\kappa}) - \mathbf{G}(-\mathbf{1}) \right) \frac{\partial \mathbf{Q}}{\partial L} \mathbf{Q}^T \right] \quad (26)$$

and contains all disorder contributions. The corresponding scaling function reads

$$\vartheta^{(\text{ex})}(\rho) = \lim_{L, M \rightarrow \infty} -\frac{L}{4} \text{Tr} \left[ \left( \langle \mathbf{G}(\boldsymbol{\kappa}) \rangle_{\kappa} - \mathbf{G}(-\mathbf{1}) \right) \frac{\partial \mathbf{Q}}{\partial L} \mathbf{Q}^T \right]. \quad (27)$$

Note that the ensemble-averaged matrix  $\langle \mathbf{G}(\boldsymbol{\kappa}) \rangle_{\kappa}$  is skew-circulant and skew-symmetric for every well defined ensemble, therefore having only  $M/2$  independent matrix elements.

In order to precisely calculate the excess Casimir force scaling function (27), reducing finite-size corrections becomes necessary. For that, the trace is taken over the eigenvalues

$$\vartheta^{(\text{ex})}(\rho) = \lim_{L, M \rightarrow \infty} -\frac{L}{4} \text{Tr} \left[ \left( \lambda_{\langle \mathbf{G}(\boldsymbol{\kappa}) \rangle_{\kappa}} - \lambda_{\mathbf{G}(-\mathbf{1})} \right) \frac{\partial \lambda_{\mathbf{Q}}}{\partial L} \lambda_{\mathbf{Q}^T} \right] \quad (28)$$

since all matrices can be diagonalized with (B.1). Next, the thermodynamic limit  $L, M \rightarrow \infty$  is taken for the disorder-independent part  $\frac{\partial \lambda_{\mathbf{Q}}}{\partial L} \lambda_{\mathbf{Q}^T}$  which leads to

$$\vartheta^{(\text{ex})}(\rho) = \lim_{L, M \rightarrow \infty} \sum_{\mu} -\frac{2\pi\mu\rho}{\cosh^2(\pi\mu\rho)} \frac{z}{1+z^2 \tanh^2(\pi\mu\rho)} \text{Im} \left( \lambda_{\langle \mathbf{G}(\boldsymbol{\kappa}) \rangle_{\kappa}} - \lambda_{\mathbf{G}(-\mathbf{1})} \right). \quad (29)$$

Note that the eigenvalues  $\lambda_{\mathbf{G}(\boldsymbol{\kappa})}$  of every  $\mathbf{G}$  is purely imaginary.

Then, the disorder averaged Casimir force scaling function is given by

$$\vartheta^{(\text{o}, \uparrow)}(\rho) = \vartheta^{(\text{o}, \downarrow)}(\rho) + \vartheta^{(\text{ex})}(\rho). \quad (30)$$

For the staggered case, it reads

$$\vartheta^{(\text{o}, \uparrow)}(\rho) = \vartheta^{(\text{o}, \text{o})}(\rho) = \frac{\pi\rho}{12} \left( \Theta_4^4(e^{-2\pi\rho}) - \Theta_2^4(e^{-2\pi\rho}) \right), \quad (31)$$

as derivative of the Casimir amplitude for open boundaries (20), with elliptic theta constants  $\Theta_2(q) = 2 \sum_{n=0}^{\infty} (-1)^n q^{(n+1/2)^2}$  and  $\Theta_4(q) = 1 + 2 \sum_{n=1}^{\infty} q^{n^2}$ .

## 2.5 Algorithms

In order to simulate the with  $M$  exponentially increasing many systems, two kinds of algorithms can be used. One algorithm based on the Sherman-Morrison-Woodbury identity [37] is used to calculate the free energy and the Casimir force for all systems, whereas the principal minor algorithm [26] is faster, but limited to free energy calculations. In comparison to calculating each determinant, which would have complexity  $\mathcal{O}(M^3 2^M)$ , both algorithms are considerably faster, with complexities  $\mathcal{O}(M^2 2^M)$  for the Woodbury method, and  $\mathcal{O}(M 2^M)$  for the principal minor algorithm, respectively.

Both methods were implemented in C/C++ on CPUs [19–21], and the principal minor algorithm has also been implemented on GPUs using TensorFlow [22]. However, due to the required high numerical precision, even with 6 NVIDIA Tesla V100S GPUs the calculations took approximately the same time as with two AMD EPYC 7742 64-Core processors.

### 2.5.1 Woodbury algorithm

Instead of calculating the determinant  $\det(\mathbf{Q} + \boldsymbol{\kappa})$  repeatedly for each  $\vec{\epsilon}$ , the idea is to update the determinant consecutively based on its previous value using the Woodbury identity [37]. One update should correspond to a single boundary spin flip and every system should be calculated exactly once. These requirements are fulfilled by using the Gray code sequence [38] as boundary spins  $\vec{\epsilon}$ , which is a binary sequence that forms a Hamiltonian cycle while changing only one spin in each step.

By flipping one boundary spin  $\epsilon_i$  at position  $i$ , the elements  $\kappa_{i-1}$  and  $\kappa_i$  will change, leading to a slightly changed matrix  $\tilde{\boldsymbol{\kappa}}$ . The free energy difference of one update is then given by

$$\Delta F(L, M; \vec{\kappa}) = -\frac{1}{2} \log \det \frac{\mathbf{Q} + \tilde{\boldsymbol{\kappa}}}{\mathbf{Q} + \boldsymbol{\kappa}} \quad (32)$$

$$= -\frac{1}{2} \log \det \left( \mathbf{1} + \frac{1}{2} (\tilde{\boldsymbol{\kappa}} - \boldsymbol{\kappa}) \mathbf{G}(\boldsymbol{\kappa}) \right), \quad (33)$$

where the matrix  $\frac{1}{2} (\tilde{\boldsymbol{\kappa}} - \boldsymbol{\kappa})$  is -1 at positions  $(i-1, i-1)$  and  $(i, i)$ , and 0 elsewhere. Therefore the determinant can be reduced to a  $2 \times 2$  minor by a Laplace expansion,

$$\Delta F(L, M; \vec{\kappa}) = -\log(\boldsymbol{\kappa} \mathbf{G}(\boldsymbol{\kappa}))_{i-1, i}, \quad (34)$$

where the skew symmetry of  $\mathbf{G}(\boldsymbol{\kappa})$  simplifies the determinant to only the  $(i-1, i)$  element of  $\mathbf{G}(\boldsymbol{\kappa})$ .

For an efficient update of  $\mathbf{G} \mapsto \tilde{\mathbf{G}} = \mathbf{G} + \Delta \mathbf{G}$  the Woodbury identity is used. Due to the skew symmetry of  $\mathbf{G}$ , the rank-2 update of  $\mathbf{G}$  can be considerably simplified. Defining the  $M \times 1$  row vector  $|\mathbf{g}_m\rangle$  as the  $m$ -th row of the matrix  $\mathbf{1} + \mathbf{G}$ , the increment  $\Delta \mathbf{G}$  is simply given by

$$\Delta \mathbf{G} = \frac{|\mathbf{g}_i\rangle \langle \mathbf{g}_{i-1}| - |\mathbf{g}_{i-1}\rangle \langle \mathbf{g}_i|}{(\mathbf{G})_{i-1, i}}. \quad (35)$$

The Casimir force (23) is updated in a similar fashion according to  $\mathcal{F}_C \mapsto \tilde{\mathcal{F}}_C = \mathcal{F}_C + \Delta \mathcal{F}_C$ , with increment

$$\Delta \mathcal{F}_C = -\frac{1}{4M} \text{Tr} \left[ \Delta \mathbf{G} \mathbf{Q}^T \frac{\partial \mathbf{Q}}{\partial L} \right]. \quad (36)$$

### 2.5.2 Principal minor algorithm

The principal minor algorithm is based on the publication by Griffin and Tsatsomeros [26] and calculates the  $2^M$  principal minors of a given  $M \times M$  matrix in  $\mathcal{O}(M2^M)$  operations. By using  $\mathbf{G}(\mathbf{1})$ , the algorithm calculates its principal minors which correspond directly to the update increments for the free energy (32). To avoid the Pivot-corrections mentioned in [26], we can use in our case the Schur-complement of  $\mathbf{G}(\mathbf{1})$  to get the same free energy increments in less computation time.

### 3 Results

#### 3.1 Free energy histograms

We start with a motivation for log-normal form: Define the marginal distribution of the residual excess free energy DOTS  $\delta\omega^{(\text{ex})}$ ,

$$\delta\omega^{(\text{ex})}(L, M; \delta F^{(\text{ex})}) = \int dM_B \delta\omega^{(\text{ex})}(L, M; \delta F^{(\text{ex})}, M_B) \quad (37)$$

$$\delta\bar{F}^{(\text{ex})}(L, M) = \int d\delta F^{(\text{ex})} \delta F^{(\text{ex})} \delta\omega^{(\text{ex})}(L, M; \delta F^{(\text{ex})}). \quad (38)$$

We know that

$$\Delta_C^{(\text{ex})}(\rho) \simeq \langle \delta F^{(\text{ex})}(L, M; \vec{\kappa}) \rangle_\kappa \quad (39)$$

is universal. We now assume that the scaling form of the DOTS  $\delta\omega^{(\text{ex})}(L, M; \delta F^{(\text{ex})})$  is universal, too.

Numerical evidence shows that  $-F^{(\text{ex})}/M$  (and therefore also  $-\delta F^{(\text{ex})}/M$ ) is asymptotically log-normal distributed, with cutoff  $f_0$ , and that the width scales like  $\sigma(M) \simeq \sigma_0/(f_1 M)^{1/2}$ , such that

$$\delta\omega^{(\text{ex})}(L, M; \delta F^{(\text{ex})}) \simeq \frac{1}{f_2 M} \mathcal{LN}\left(\mu(L, M), \sigma(M); \frac{f_0 - \delta F^{(\text{ex})}/M}{f_2}\right), \quad (40)$$

with yet unknown constants  $f_{1,2}$ . The first moment of  $\mathcal{LN}(\mu, \sigma; x)$  is known to be  $\langle x \rangle = e^{\mu + \sigma^2/2}$ . Expanding around  $M = \infty$  and comparing to the scaling prediction (39) leads to the conclusion that  $\mu(L, M) \simeq \mu_0(\rho)/(f_1 M)$ , with constants  $f_2 = f_1 = f_0$ , such that the resulting scaling form reads

$$\delta\omega^{(\text{ex})}(L, M; \delta F^{(\text{ex})}) \simeq \frac{1}{f_0 M} \mathcal{LN}\left(\frac{\mu_0(\rho)}{f_0 M}, \frac{\sigma_0}{\sqrt{f_0 M}}; 1 - \frac{\delta F^{(\text{ex})}}{f_0 M}\right), \quad (41)$$

and the excess Casimir amplitude becomes

$$\Delta_C^{(\text{ex})}(\rho) = -\left(\mu_0(\rho) + \frac{1}{2}\sigma_0^2\right). \quad (42)$$

The remaining unknown  $f_0$  can be adjusted to compensate for remaining leading order corrections. For  $\rho = \infty$  we find  $f_0 = 0.07(?)$ .

#### 3.2 Critical random surface free energy

For the determination of the leading surface divergence  $\bar{f}_s^{(r)}M$  from (14), we calculate the finite difference of (9a) in  $M$ , leading to a sequence converging towards

$$f_s^{(\text{ex})} = \bar{f}_s^{(r)} - f_s^{(\downarrow)} = \lim_{M \rightarrow \infty} \frac{\bar{F}^{(\text{ex})}(L \rightarrow \infty, M+1) - \bar{F}^{(\text{ex})}(L \rightarrow \infty, M-1)}{2} \quad (43)$$

in the thermodynamic limit. Note that here  $L \rightarrow \infty$  is used as these semi-infinite systems show the smallest lattice corrections.

When using a sequence  $a_n$  of exactly calculated values, the convergence can be accelerated with for example Aitken's delta squared process [39]

$$S[a_n] = \frac{a_{n+1}a_{n-1} - a_n^2}{a_{n+1} - 2a_n + a_{n-1}} \quad (44)$$

or the Levin-U transform [40]

$$u_{k,b}^{(n)}[a_n] = \frac{\sum_{j=0}^k (-1)^j \binom{k}{j} \frac{(b+n+j)^{k-2}}{(b+n+k)^{k-1}} \frac{a_{n+j}}{a_{n+j}-a_{n-1+j}}}{\sum_{j=0}^k (-1)^j \binom{k}{j} \frac{(b+n+j)^{k-2}}{(b+n+k)^{k-1}} \frac{1}{a_{n+j}-a_{n-1+j}}}, \quad (45)$$

where we use in the following  $b = 1$ , and  $k$  up to  $k = 12$ .

Another method to get closer to the limit is by canceling out higher order corrections. By assuming that these corrections follow some type of Taylor expansion like  $\sum_i \frac{c_i}{M^i}$  in the limit  $M \rightarrow \infty$ , the  $k$ -th term can be canceled out by applying the generalized difference operator

$$\Psi_k[a_n] = \frac{(n-1)^k a_{n+1} - (n+1)^k a_{n-1}}{(n-1)^k - (n+1)^k} \quad (46)$$

to the sequence  $a_n$ . Note that in terms of free energy,  $a_n = F(M)$  and  $n = M$ . Also, equation (43) can be expressed as  $\Psi_0[\bar{F}^{(\text{ex})}(L \rightarrow \infty, M)]$ .

In order to determine the surface free energy densities  $f_s$  shown in table 1, the computed free energies are either extrapolated with a classical fit method or with one of the three methods (44), (45), (46) mentioned before.

We find  $\bar{f}_s^{(r)} = f_s^{(m_B=0)}$ , where the deviation between different methods is slightly larger in the  $(o, m_B = 0)$  ensemble than in the ensemble  $(o, r)$ . Also, the surface free energy density in the hamiltonian limit  $z_c \rightarrow 1$  is about 100 times larger as in the isotropic case.

Table 1: Surface free energy densities calculated with before mentioned methods. Note that the mean for  $f_s^{(m_B=0)}(z_c^{\text{iso}})$  is taken only over the  $\Psi$ -Method and the Levin-U transform value. For  $\bar{f}_s^{(r)}(z_c^{\text{iso}})$ , we neglected the classical fit value, as in both cases the not included methods have too large error margins to be representative. Further, we come to the conclusion  $f_s^{(m_B=0)}(z_c^{\text{iso}}) = \bar{f}_s^{(r)}(z_c^{\text{iso}})$ .

	$\bar{f}_s^{(r)}(z_c^{\text{iso}})$	$f_s^{(m_B=0)}(z_c^{\text{iso}})$	$\lim_{z_c \rightarrow 1} \bar{f}_s^{(r)}(z_c)$
mean	0.002662(25 ± 28)	0.00266(42 ± 20)	0.26536(96 ± 10)
classical fit	0.00266(11 ± 30)	0.002(71 ± 12)	0.26536(91 ± 32)
$\Psi$ -Method + fit	0.002662(6 ± 7)	0.00266(48 ± 24)	0.26537(08 ± 22)
Aitken's	0.002662(10 ± 18)	0.0026(5 ± 6)	0.265369(2 ± 7)
Levin-U	0.002662(0 ± 4)	0.00266(37 ± 32)	0.265369(15 ± 33)
maximum $M$	48	48	54

### 3.3 The Casimir amplitude

The computationally obtained free energies can be transformed with the operator  $\Psi$  to a sequence that converges towards the Casimir amplitude

$$\lim_{L, M \rightarrow \infty} \Psi_1[\bar{F}^{(\text{ex})}(L, M)] = \Delta_C^{(\text{ex})}(\rho) \quad (47)$$

in the thermodynamic limit with the advantage that the surface divergence cancels out exactly.

Further, the four methods classical fit, Aitken transform (44), Levin-U transform (45) and a combination of the  $\Psi$ -method (46) and fit are used to calculate the Casimir amplitudes for different ensembles.

In figure 3, the excess Casimir amplitude (18) is plotted in dependence of aspect ratio  $\rho$ . The values from different methods scatter around zero, where the deviation shows a minor logarithmic dependence on  $\rho$ . Most likely, this is an error occurring from finite-size effects

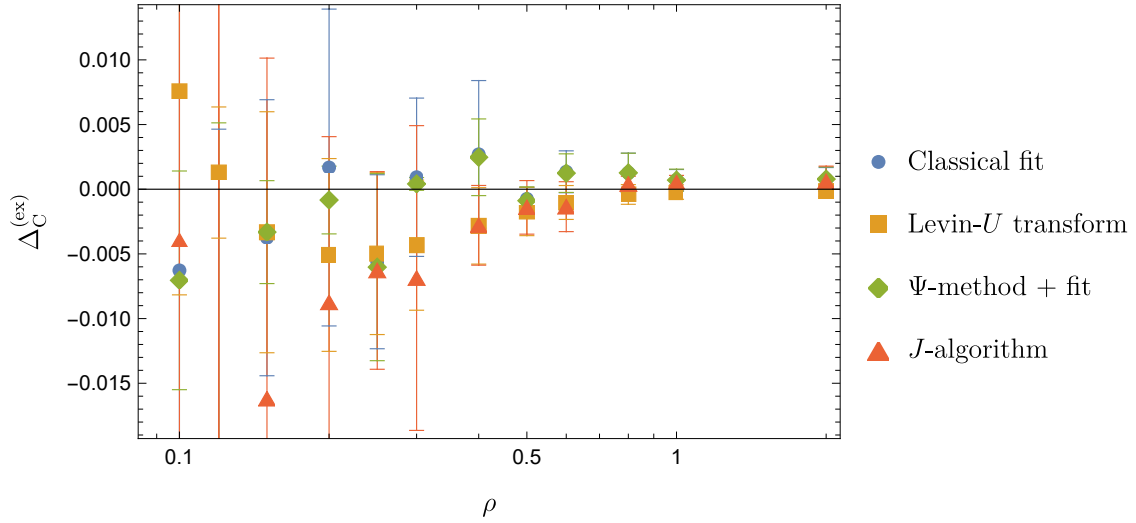


Figure 3: Excess Casimir amplitude (18)

for small  $\rho = L/M$  and  $L$  as  $M$  is fixed due to the computation time. Further, Diehl and Nüsser [41] derived a Harris criterion for surfaces with conclusion that surface disorder with mean zero becomes irrelevant in the Ising universality class for arbitrary dimensions  $d \neq 2$ . For the case  $d = 2$ , there could not be made a prediction, but our data 3 lead to the hypothesis that  $\Delta_C^{(\text{ex})}(\rho) \equiv \Delta_C^{(o,r)}(\rho) - \Delta_C^{(o,o)}(\rho) = 0$ .

For  $\rho \rightarrow \infty$ , we find for isotropic couplings

$$z_c = z_c^{\text{iso}} : \lim_{\rho \rightarrow \infty} \Delta_C^{(\text{ex})}(\rho) = (2.8 \pm 5) \times 10^{-4} \quad (48)$$

and in the hamiltonian limit

$$z_c \rightarrow 1 : \lim_{\rho \rightarrow \infty} \Delta_C^{(\text{ex})}(\rho) = (1.9 \pm 3) \times 10^{-5} \quad (49)$$

via combination of  $\Psi$ -method and fit. Note that the Casimir amplitude is a universal quantity and therefore cannot depend on the coupling. Rather, both Casimir amplitudes seem to be zero and the deviation occurring from finite-size effects is coupling-dependent.

### 3.4 Casimir force scaling function

Next, the Casimir force scaling function will be discussed for arbitrary  $\rho$  and different ensembles. Although the algorithm that is used to calculate the force, is slower than for the free energy and thus reducing the maximum system size to  $M = 40$ , we achieved roughly the same precision for the Casimir force scaling function due to an analytic reduction of finite-size effects, see (29). The determination of Casimir force scaling functions  $\vartheta$  is done again via combination of  $\Psi$ -method and fit. Figure 4a shows  $\vartheta^{(o,r)}$  and  $\vartheta^{(o,m_B=0)}$ , with analytic known  $\vartheta^{(o,o)}$  (31) as reference.

The deviation of  $\vartheta^{(o,r)}$  from  $\vartheta^{(o,o)}$  is again visible for small  $\rho \lesssim 0.3$  and should be an error, resulting from finite-size effects. The force scaling function for the ensemble  $(o, m_B = 0)$  deviates more from  $\vartheta^{(o,o)}$  as  $\vartheta^{(o,r)}$ . On the one hand, the ensemble already showed larger finite-size corrections for the surface free energy density (1), which makes it likely that this deviation is in fact an error that cannot be estimated. On the other hand, this could be a new surface universality class as the ensemble  $(o, r)$  can be imagined as a grand canonical ensemble, whereas the ensemble  $(o, m_B = 0)$  would represent a canonical ensemble.

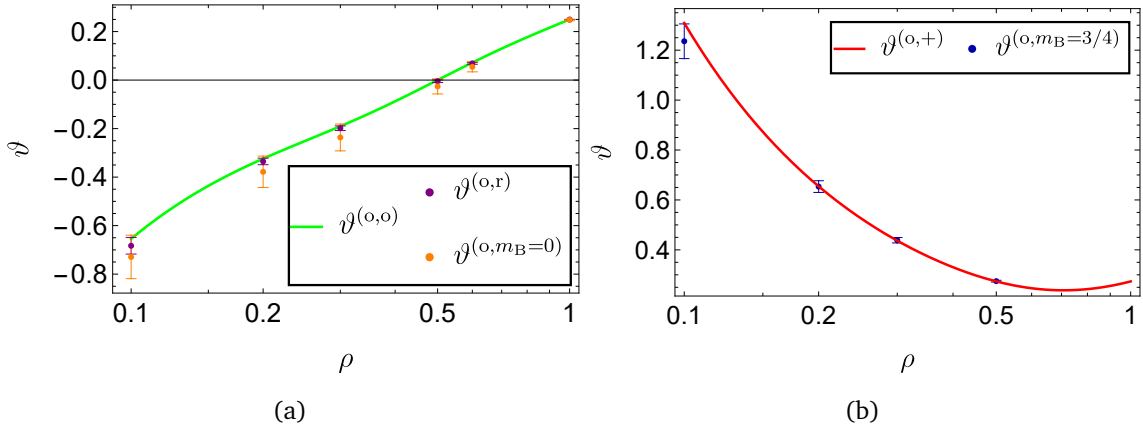


Figure 4: The dots represent Casimir force scaling functions that are calculated with the  $\Psi$ -method. Lines are analytically known scaling functions.

Additionally, we find the sign change of the Casimir force scaling function at  $\rho_0^{(o,m_B=0)} \approx 0.52$ , in comparison to the open cylinder  $\rho_0^{(o,o)} = \rho_0^{(o,r)} = 1/2$ . The Casimir force scaling function for the ensemble  $(o, m_B = 3/4)$  is shown in figure 4b. As predicted from field theory, the scaling function  $\vartheta^{(o,m_B=3/4)}$  seems to be in the  $(o, +)$  universality class in realm of the error margin. Again, there is a larger deviation for the smallest value of  $\rho = 0.1$  which is due to finite-size corrections.

## 4 Conclusion

We presented an exact solution for the free energy of a square lattice Ising cylinder with one arbitrary quenched boundary and focused our work on surface disorder effects for different couplings at criticality.

The probability density function of free energies in the disorder ensemble  $(o, r)$  of all possible boundaries turns out to behave like a log-normal distribution, a property that could also be shown recently in the framework of a random-matrix-theory approach of the same model [42]. Further, multiple quantities are calculated in the thermodynamic limit by using various sequence acceleration techniques to reduce finite-size corrections.

The surface free energy densities for the disorder ensemble  $(o, r)$  and for the ensemble  $(o, m_B = 0)$  with fixed boundary magnetization  $m_B = 0$  are shown to be equal for isotropic ( $z_c^{\text{iso}}$ ) and maximal anisotropic ( $z_c \rightarrow 1$ ) couplings with a precision of 6 digits after the decimal point.

Unlike with the free energy surface density, it turns out that the Casimir amplitude, the finite-size scaling function of the free energy, is the same for open boundaries as it is for the disorder ensemble  $(o, r)$ . Therefore, we verify the predictions from conformal field theory with our exact solution of a quenched boundary for  $\rho \rightarrow \infty$  and see slight deviations in dependence of  $\rho$ , possibly due to finite-size corrections.

At last, we proved with calculations of the Casimir force scaling function that the ensemble  $(o, m_B = 3/4)$  with fixed boundary magnetization to  $m_B = 3/4$  turns out to be equal to the boundary  $(o, +)$  of all spins pointing up on one side. Further, finite-size corrections occurred for the different ensembles for small  $\rho$ . Whereas the ensemble  $(o, r)$  shows again to be equal to  $(o, o)$ , the ensemble  $(o, m_B = 0)$  deviates in a way that there cannot be made a statement whether or not this are large finite-size corrections or if this ensemble belongs to a new universality class.

## Acknowledgements

**Funding information** This work was partially supported by the Deutsche Forschungsgemeinschaft (DFG, German Research Foundation) under project 278162697 – SFB 1242.

## A Derivation of the partition function

The partition function in (3) is based on the transfer matrix method from [14], except the transfer matrix  $\mathcal{T} = \mathbf{U}_t \mathbf{U}_z$  used here is Wick-rotated. It consists of the following  $2M \times 2M$  dimensional matrices

$$\mathbf{U}_t = \begin{pmatrix} \mathbf{H} \mathbf{t}_+ \mathbf{H}^T & i \mathbf{H}^T \mathbf{t}_- \\ -i \mathbf{t}_- \mathbf{H} & \mathbf{t}_+ \end{pmatrix}, \quad \mathbf{U}_z = \begin{pmatrix} \mathbf{z}_+ & -i \mathbf{z}_- \\ i \mathbf{z}_- & \mathbf{z}_+ \end{pmatrix}, \quad (\text{A.1})$$

which are each describing one layer of bulk couplings in  $t$ - or  $z$ - direction respectively. The  $M \times M$  diagonal matrices  $\mathbf{t}_\pm = \mathbf{diag}(t_\pm)$  and  $\mathbf{z}_\pm = \mathbf{diag}(z_\pm)$  are defined by couplings  $t$  and  $z$  and the dual transformation  $(x)_\pm = \frac{1}{2}(x \pm \frac{1}{x})$ . The  $M \times M$  matrix  $\mathbf{H}$  is given by

$$\mathbf{H} = \begin{pmatrix} 0 & 1 & 0 & \cdots & 0 \\ \vdots & \ddots & \ddots & \ddots & \vdots \\ \vdots & \ddots & \ddots & \ddots & 0 \\ 0 & \ddots & \ddots & \ddots & 1 \\ -1 & 0 & \cdots & \cdots & 0 \end{pmatrix}. \quad (\text{A.2})$$

With that, the partition function of the open cylinder is given by

$$Z^{(0,0)} = \sqrt{2^{M+1} C \det \langle \mathbf{e}_0 | \mathcal{T}^L \mathbf{U}_t | \mathbf{e}_0 \rangle} \quad (\text{A.3})$$

with constant  $C = 2^{(L+1)M-1} (-z_-)^{-LM}$  and the  $2M \times M$  boundary vector

$$|\mathbf{e}_0\rangle = \frac{1}{\sqrt{2}} \begin{pmatrix} \mathbf{1} \\ -i \mathbf{1} \end{pmatrix}, \quad (\text{A.4})$$

which describes the open surface and its effects on the bulk.

In order to get a system with a quenched boundary condition on the right, the boundary couplings  $K_{s,m}^\uparrow = \kappa_m K_s^\uparrow$  have to be infinitely strong, where each coupling sign  $\kappa_m = \pm 1$  can later be chosen independently to create arbitrary boundary conditions. For that, the corresponding limit  $\lim_{K_s^\uparrow \rightarrow \infty} \mathbf{U}_t$  has to be regularized by multiplying with  $(t_+)^{-1}$  in order to get a finite matrix

$$\lim_{K_s^\uparrow \rightarrow \infty} (t_+)^{-1} \mathbf{U}_t = 2 |\mathbf{e}_\kappa\rangle \langle \mathbf{e}_\kappa|, \quad |\mathbf{e}_\kappa\rangle = \frac{1}{\sqrt{2}} \begin{pmatrix} \mathbf{1} \\ i \kappa \mathbf{H} \end{pmatrix}. \quad (\text{A.5})$$

The new block vector  $|\mathbf{e}_\kappa\rangle$  corresponds to a quenched, arbitrary boundary condition with  $\kappa = \mathbf{diag}(\vec{\kappa})$ . Exchanging the matrix  $\mathbf{U}_t$  on the right of the transfer matrix in (A.3) with the regularized terms from (A.5), results in the partition function for an arbitrary, quenched boundary

$$Z^{(0,r)} = \sqrt{\frac{C}{2} \det \langle \mathbf{e}_0 | \mathcal{T}^L | \mathbf{e}_\kappa \rangle \det (2 \langle \mathbf{e}_\kappa | \mathbf{e}_0 \rangle)} = \sqrt{C \det \langle \mathbf{e}_0 | \mathcal{T}^L | \mathbf{e}_\kappa \rangle} \quad (\text{A.6})$$

as presented already in (3). The determinant  $\det(2\langle \mathbf{e}_\kappa | \mathbf{e}_o \rangle)$  can be identified as  $1 + \prod_{k=1}^M \kappa_m = 2$ , as the product over all  $\kappa_m$  is always one per definition. Note that from (A.3) to (A.6) are multiple changes in prefactors. Due to the quenching,  $M$  previously free spins become the arbitrary boundary which results in a reduction of the partition function by a factor of  $2^{M/2}$ . Furthermore, one arbitrary boundary condition characterized by coupling signs  $\kappa_m$ , represents not only one corresponding spin configuration but also its  $Z_2$ -symmetric one, resulting in an additional factor of  $1/2$  in the partition function to get to (A.6).

Now, further focus will be laid on rewriting (A.6) to handle the exponential growth of the elements of  $\mathcal{T}^L$  in  $L$ . Its block matrix representation

$$\mathcal{T}^L = \begin{pmatrix} \mathbf{T}_1 & i\mathbf{T}_2 \\ -i\mathbf{T}_2^T & \mathbf{T}_1^T \end{pmatrix} \quad (\text{A.7})$$

becomes useful with  $\mathbf{T}_i$  as real  $M \times M$  matrices that can be calculated analytically from (A.1). The partition function (A.6) simplifies to

$$Z^{(o,r)}(L, M; \boldsymbol{\kappa}) = \sqrt{C \det \left( \frac{\mathbf{T}_1 + \mathbf{T}_2^T}{2} - \frac{\mathbf{T}_1^T + \mathbf{T}_2}{2} \boldsymbol{\kappa} \mathbf{H} \right)} \quad (\text{A.8})$$

by carrying out the block matrix multiplications. Further simplifications lead to

$$Z^{(o,r)}(L, M; \boldsymbol{\kappa}) = \sqrt{C \det \mathbf{P} \det(\mathbf{Q} + \boldsymbol{\kappa})}, \quad (\text{A.9})$$

where the  $M \times M$  matrix  $\mathbf{P} = \frac{1}{2}(\mathbf{T}_1 + \mathbf{T}_2^T)$  still grows exponentially in  $L$ , but the matrix elements of

$$\mathbf{Q} = -\mathbf{H} \frac{\mathbf{P}^T}{\mathbf{P}} \quad (\text{A.10})$$

are in the order of one for arbitrary  $L$  and  $M$ . As the diverging determinant of  $\mathbf{P}$  is not dependent on  $\boldsymbol{\kappa}$ , one can divide the partition function by a reference partition function, to cancel out the corresponding determinant like done for the free energy in (9a).

## B Analytic calculation of matrix $\mathbf{Q}$

The derived matrix  $\mathbf{Q}$  from (A.10) is of great interest, since it connects the pure boundary condition given by  $\boldsymbol{\kappa}$  with the Ising model via  $\det(\mathbf{Q} + \boldsymbol{\kappa})$ . As  $\mathbf{Q}$  is skew-circulant, it can be diagonalized with a discrete Fourier transform, like

$$\mathcal{F} = \left[ \frac{1}{\sqrt{M}} e^{\frac{i\pi l \mu}{M}} \right]_{l=1, \mu \text{ odd}}^M, \quad (\text{B.1})$$

where  $\mu$  runs here and in the following over the odd integers between  $-M$  and  $M$ . The analytical calculation of  $\mathbf{Q}$  from (A.10) leads to its eigenvalues

$$\lambda_{\mathbf{Q}, \mu} = (\mathcal{F}^\dagger \mathbf{Q} \mathcal{F})_{\mu, \mu} = -e^{i\varphi} \frac{1 + (\sin \omega + iz \cos \omega) \tanh(L\gamma)}{1 + (\sin \omega - iz \cos \omega) \tanh(L\gamma)} \quad (\text{B.2})$$

for even  $M$  and arbitrary  $L = \frac{1}{-z_-} \rho M > 0$ . The three angles introduced in (B.2) are all dependent on  $\mu$  and given by

$$\gamma = \text{sgn}(\varphi) \text{arccosh}(t_+ z_+ - t_- z_- \cos \varphi) \quad (\text{B.3})$$

$$\omega = \arctan\left(\frac{t_+ z_- - t_- z_+ \cos \varphi}{t_- \sin \varphi}\right) \quad (\text{B.4})$$

$$\varphi = \frac{\pi \mu}{M}. \quad (\text{B.5})$$

The hyperbolic angle  $\gamma$  is linked to the eigenvalues  $\lambda_{\mathcal{T},\mu} = e^\gamma$  of transfer matrix  $\mathcal{T}$  and via the Onsager dispersion relation  $\cosh \gamma + t_- z_- \cos \varphi = t_+ z_+$  to angle  $\varphi$ . The latter one is connected to the eigenvalues of a transfer matrix that would propagate in  $\downarrow$ -direction [14], where the definition from (B.3) is only valid for the cylindrical geometry. For the Ising rectangle, it is given in [16]. The definition of  $\omega$  serves aesthetic purpose and fulfills the relation  $i \tan \omega = \cosh \theta$ , with  $\theta$  as relevant angle for the Ising rectangle [16].

For the hamiltonian limit  $\lim_{t,z \nearrow 1} \mathbf{Q}$  has to be series expanded around  $\delta \rightarrow 0$ , with  $t, z = 1 - \delta$ , leading to

$$\lim_{\delta \rightarrow 0} \lambda_{\mathbf{Q},\mu} = \frac{e^{i\varphi} + ie^{i\frac{\varphi}{2}} \tanh(2\rho M \sin \frac{\varphi}{2})}{-1 + ie^{i\frac{\varphi}{2}} \tanh(2\rho M \sin \frac{\varphi}{2})} + \mathcal{O}(\delta)^2. \quad (\text{B.6})$$

In order to calculate the critical Casimir force in (26), the derivative  $\frac{\partial \mathbf{Q}}{\partial L}$  is needed, which can be expressed as

$$\frac{\partial \lambda_{\mathbf{Q},\mu}}{\partial L} = \left( \mathcal{F}^\dagger \frac{\partial \mathbf{Q}}{\partial L} \mathcal{F} \right)_{\mu,\mu} = \frac{2ie^{i\varphi} \gamma z \cos \omega}{\cosh^2(L\gamma)} \left( \frac{1}{i + (i \sin \omega + z \cos \omega) \tanh(L\gamma)} \right)^2 \quad (\text{B.7})$$

for arbitrary  $t, z$  and as

$$\lim_{\delta \rightarrow 0} L \frac{\partial \lambda_{\mathbf{Q},\mu}}{\partial L} = \frac{2i\rho M e^{i\varphi} \sin \varphi}{\cosh^2(2\rho M \sin \frac{\varphi}{2})} \left( \frac{1}{i + e^{i\frac{\varphi}{2}} \tanh(2\rho M \sin \frac{\varphi}{2})} \right)^2 + \mathcal{O}(\delta)^2 \quad (\text{B.8})$$

for the Hamiltonian limit. Note that the eigenvalue  $\frac{\partial \lambda_{\mathbf{Q},\mu}}{\partial L}$  has to be multiplied with  $L$  first before taking the limit, in order to get a finite result.

## References

- [1] E. Ising, *Beitrag zur Theorie des Ferromagnetismus*, Z. Phys. **31**, 253 (1925).
- [2] L. Onsager, *Crystal statistics. I. A two-dimensional model with an order-disorder transition*, Phys. Rev. **65**, 117 (1944), doi:[10.1103/PhysRev.65.117](https://doi.org/10.1103/PhysRev.65.117).
- [3] B. Kaufman, *Crystal statistics. II. Partition function evaluated by spinor analysis*, Phys. Rev. **76**(8), 1232 (1949), doi:[10.1103/PhysRev.76.1232](https://doi.org/10.1103/PhysRev.76.1232).
- [4] P. W. Kasteleyn, *The statistics of dimers on a lattice: I. The number of dimer arrangements on a quadratic lattice*, Physica **27**(12), 1209 (1961), doi:[10.1016/0031-8914\(61\)90063-5](https://doi.org/10.1016/0031-8914(61)90063-5).
- [5] P. W. Kasteleyn, *Dimer statistics and phase transitions*, J. Math. Phys. **4**, 287 (1963).
- [6] M. E. Fisher, *On the dimer solution of planar Ising models*, Journal of Mathematical Physics **7**(10), 1776 (1966), doi:[10.1063/1.1704825](https://doi.org/10.1063/1.1704825).

- [7] B. M. McCoy and T. T. Wu, *The Two-Dimensional Ising Model*, Harvard University Press, Cambridge (1973).
- [8] B. M. McCoy and T. T. Wu, *The Two-Dimensional Ising Model*, Dover Books on Physics. Dover Publication, Inc., Mineola, New York (2014).
- [9] M. E. Fisher and P.-G. de Gennes, *Phénomènes aux parois dans un mélange binaire critique*, C. R. Acad. Sci. Paris, Ser. B **287**, 207 (1978).
- [10] H. B. G. Casimir, *On the attraction between two perfectly conducting plates*, Proc. K. Ned. Akad. Wet. **51**, 793 (1948).
- [11] A. Gambassi, *The Casimir effect: From quantum to critical fluctuations*, Journal of Physics: Conference Series **161**(1), 012037 (2009), doi:[10.1088/1742-6596/161/1/012037](https://doi.org/10.1088/1742-6596/161/1/012037).
- [12] D. Dantchev and S. Dietrich, *Critical casimir effect: Exact results*, Physics Reports **1005**, 1 (2023), doi:<https://doi.org/10.1016/j.physrep.2022.12.004>, Critical Casimir Effect: Exact Results.
- [13] R. J. Baxter, *The bulk, surface and corner free energies of the square lattice Ising model*, J. Phys. A: Math. Theor. **50**(1), 014001 (2017), doi:[10.1088/1751-8113/50/1/014001](https://doi.org/10.1088/1751-8113/50/1/014001), arXiv:1606.02029.
- [14] A. Hucht, *The square lattice Ising model on the rectangle I: finite systems*, J. Phys. A: Math. Theor. **50**(6), 065201 (2017), doi:[10.1088/1751-8121/aa5535](https://doi.org/10.1088/1751-8121/aa5535), [1609.01963](https://arxiv.org/abs/1609.01963).
- [15] A. Hucht, *The square lattice Ising model on the rectangle II: finite-size scaling limit*, J. Phys. A: Math. Theor. **50**(26), 265205 (2017), doi:[10.1088/1751-8121/aa6b7a](https://doi.org/10.1088/1751-8121/aa6b7a), [1701.08722](https://arxiv.org/abs/1701.08722).
- [16] A. Hucht, *The square lattice Ising model on the rectangle III: Hankel and Toeplitz determinants*, J. Phys. A: Math. Theor. **54**(26), 375201 (2021), doi:[10.1088/1751-8121/ac0983](https://doi.org/10.1088/1751-8121/ac0983), [2103.10776](https://arxiv.org/abs/2103.10776).
- [17] E. Vernier and J. L. Jacobsen, *Corner free energies and boundary effects for Ising, Potts and fully-packed loop models on the square and triangular lattices*, J. Phys. A: Math. Theor. **45**, 045003 (2012), doi:[10.1088/1751-8113/45/4/045003](https://doi.org/10.1088/1751-8113/45/4/045003), ArXiv:1110.2158.
- [18] L. G. Molinari, *Determinants of block tridiagonal matrices*, Linear Algebra Appl. **429**, 2221 (2008), doi:[10.1016/j.laa.2008.06.015](https://doi.org/10.1016/j.laa.2008.06.015), arXiv:0712.0681.
- [19] J. Büddefeld, *Entwicklung eines Bondflip-Algorithmus für das zweidimensionale, ungeordnete Isingmodell*, Masterarbeit, Universität Duisburg-Essen (2020).
- [20] L. Cervellera, *Einfluss von Oberflächen-Unordnung auf den kritischen Casimir-Effekt*, Bachelorarbeit, Universität Duisburg-Essen (2020).
- [21] L. Cervellera, *Surface Disorder in the Two-Dimensional Ising Model*, Masterarbeit, Universität Duisburg-Essen (2022).
- [22] O. Oing, *Exakte Berechnung von Unordnungsmittelwerten im 2D-Isingmodell mit GPUs*, Bachelorarbeit, Universität Duisburg-Essen (2023).
- [23] J. L. Cardy, *The Ising model in a random boundary field*, J. Phys. A Math. Gen. **24**(22), L1315 (1991).

- [24] H. W. Diehl, *The theory of boundary critical phenomena*, Int. J. Mod. Phys. B **11**(30), 3503 (1997).
- [25] M. Pleimling, F. A. Bagaméry, L. Turban and F. Iglói, *Logarithmic corrections in the two-dimensional Ising model in a random surface field*, J. Phys. A Math. Gen. **37**(37), 8801 (2004).
- [26] K. Griffin and M. J. Tsatsomeros, *Principal minors, Part I: A method for computing all the principal minors of a matrix*, Linear Algebra Appl. **419**(1), 107 (2006).
- [27] F. Šimkovic IV and M. Ferrero, *Fast principal minor algorithms for diagrammatic Monte Carlo*, Phys. Rev. B **105**, 125104 (2022), doi:[10.1103/PhysRevB.105.125104](https://doi.org/10.1103/PhysRevB.105.125104).
- [28] H. Hobrecht and A. Hucht, *Anisotropic scaling of the two-dimensional Ising model II: surfaces and boundary fields*, SciPost Phys. **8**, 32 (2020), doi:[10.21468/SciPostPhys.8.3.032](https://doi.org/10.21468/SciPostPhys.8.3.032), [1805.00369](https://arxiv.org/abs/1805.00369).
- [29] H. A. Kramers and G. H. Wannier, *Statistics of the two-dimensional ferromagnet. Part I*, Phys. Rev. **60**, 252 (1941), doi:[10.1103/PhysRev.60.252](https://doi.org/10.1103/PhysRev.60.252).
- [30] M. Henkel, *Conformal Invariance and Critical Phenomena*, Texts and Monographs in Physics. Springer-Verlag, Berlin Heidelberg (1999).
- [31] L. Radzihovsky, *Physics 7240: Advanced statistical mechanics lecture 7: Introduction to quenched disorder* (2017).
- [32] R. J. Baxter, *Exactly Solved Models in Statistical Mechanics*, Academic Press, London (1982).
- [33] H. Hobrecht and A. Hucht, *Anisotropic scaling of the two-dimensional Ising model I: the torus*, SciPost Phys. **7**, 26 (2019), doi:[10.21468/SciPostPhys.7.3.026](https://doi.org/10.21468/SciPostPhys.7.3.026), [1803.10155](https://arxiv.org/abs/1803.10155).
- [34] R. Evans and J. Stecki, *Solvation force in two-dimensional Ising strips*, Phys. Rev. B **49**, 8842 (1994), doi:[10.1103/PhysRevB.49.8842](https://doi.org/10.1103/PhysRevB.49.8842).
- [35] H. Hobrecht and A. Hucht, *Critical Casimir force scaling functions of the two-dimensional Ising model at finite aspect ratios*, J. Stat. Mech.: Theory Exp. **2017**, 024002 (2017), doi:[10.1088/1742-5468/aa5280](https://doi.org/10.1088/1742-5468/aa5280), [1611.05622](https://arxiv.org/abs/1611.05622).
- [36] H. Hobrecht and A. Hucht, *Many-body critical Casimir interactions in colloidal suspensions*, Phys. Rev. E **92**, 042315 (2015), doi:[10.1103/PhysRevE.92.042315](https://doi.org/10.1103/PhysRevE.92.042315).
- [37] J. Sherman and W. J. Morrison, *Adjustment of an Inverse Matrix Corresponding to a Change in One Element of a Given Matrix*, The Annals of Mathematical Statistics **21**(1), 124 (1950), doi:[10.1214/aoms/1177729893](https://doi.org/10.1214/aoms/1177729893).
- [38] Wikipedia contributors, *Gray code — Wikipedia, the free encyclopedia*, [Online; accessed 24-August-2024] (2024).
- [39] A. C. Aitken, *On Bernoulli's numerical solution of algebraic equations*, Proceedings of the Royal Society of Edinburgh **46**, 289–305 (1927), doi:[10.1017/S0370164600022070](https://doi.org/10.1017/S0370164600022070).
- [40] D. Levin, *Development of non-linear transformations for improving convergence of sequences*, International Journal of Computer Mathematics **3**(1-4), 371 (1972), doi:[10.1080/00207167308803075](https://doi.org/10.1080/00207167308803075), <https://doi.org/10.1080/00207167308803075>.

- 
- [41] H. Diehl and A. Nüßer, *Critical behavior at dirty surfaces*, *Zeitschrift für Physik B Condensed Matter* **79**(1), 69 (1990).
- [42] N. Gluth, T. Guhr and A. Hucht, *Random matrices and the free energy of Ising-like models with disorder*, *SciPost Phys.* (2024).